

# Simulation of the Penetration Rate Effects of ACC and CACC on Macroscopic Traffic Dynamics

Anargiros I. Delis<sup>1</sup>, Ioannis K. Nikolos<sup>2</sup> and Markos Papageorgiou<sup>3</sup>

**Abstract**—A macroscopic approach modeling the penetration rate of Adaptive Cruise Control (ACC) and Cooperative Adaptive Cruise Control (CACC) vehicles and its effect on traffic dynamics is investigated. Modeling is based on the introduction of a relaxation term in a gas-kinetic traffic flow (GKT) model that satisfies the time-gap principle of ACC or CACC systems and allows for consideration of mixed traffic of manual and ACC/CACC vehicles. The relaxation time is assigned to multiple leading vehicles in the CACC case; whereas in the ACC case only relates to the direct leading vehicle. Numerical simulations investigate the effect of the penetration rates of ACC and CACC equipped vehicles to traffic flow macroscopic stability, with respect to perturbations introduced in a ring road, and to flow characteristics in an open freeway with merging flow at an on-ramp.

## I. INTRODUCTION

Vehicle control systems such as Adaptive Cruise Control (ACC) and Cooperative Adaptive Cruise Control (CACC) could potentially have significant impacts on traffic flow in the near future. Accurate models of the traffic flow implications of both of these systems are in need so as to enable realistic predictions of their effects on highway capacity and traffic dynamics. In an ACC system, a set speed can be chosen using the driver interface but when a leading vehicle is detected by its sensors its speed is adapted to that of the leading vehicle based on a pre-selected time gap. Thus, the driver is liberated from the need to adjust its speed to that of the leader under regular traffic conditions. However, the application of ACC systems, for certain parameter settings, may also induce some negative effects on traffic dynamics. The next generation of longitudinal control systems is now focused on adding vehicle-to-vehicle (V2V) communications to take advantage of more extensive information from multiple preceding vehicles. V2V CACC systems have such ability of sharing traffic information via vehicular networks or wireless technologies so then an equipped vehicle can potentially follow its predecessor with higher accuracy, faster response and shorter gaps. ACC systems are available in the market, mainly on premium vehicles, but with some introductions on middle-class vehicles as well. Hence, it is of interest to study the effects of different penetration rates of such systems in various flow conditions. Although much work has been reported for the microscopic simulation of ACC/CACC systems, we refer for example to [5], [3],

[11], [12] and references therein, model development at the macroscopic traffic flow level for the simulation of such systems are relatively rare. Very recently, and closely related to the present work, in [6], [8], [7], [2], [9], [10] macroscopic models were proposed to describe the operations of ACC and CACC in the traffic flow. In these works it was found that at a 100% penetration, CACC reduced traffic congestion by improving highway capacity and throughput and attenuated traffic flow instabilities to a greater extent compared to ACC. The present work aims to contribute to the macroscopic modeling of mixed traffic of manual and ACC or CACC vehicles and it builds on a previous work of the authors in [2], [9]. It is noted that in [2], [9] only the case of a 100% penetration rate was considered for both ACC and CACC flows. Here, the GKT second-order traffic flow model, [13], [4], [14], is again utilized as a basis to import and access the macroscopic simulation of ACC/CACC traffic. ACC and CACC effects are incorporated as source terms to the second (“flow”) equation of the system of partial differential equations forming the GKT model, which controls the speed dynamics. In our modeling approach the time-gap parameter, which is an important characteristic of such systems, is explicitly taken into account. The main contributions of the present work can be summarized as: (a) to incorporate macroscopically the penetration rate of ACC or CACC equipped vehicles in the GKT model and (b) to qualitatively assess, through numerical simulations, various traffic flow scenarios for mixed manually driven and ACC or CACC equipped vehicles.

## II. MACROSCOPIC MODELLING FOR ACC/CACC

We extend here the gas-kinetic-based traffic (GKT) flow model from [13], [4], [14], [2], [9], written in conservation law form with source terms as

$$\partial_t \rho + \partial_x q = r_{rmp}; \quad (1)$$

$$\partial_t q + \partial_x (\rho u^2 + \theta \rho) = \rho \left( \frac{V_e^*(\rho) - u}{\tau} \right) [1 - pF(\rho)] + h_{rmp} + p\mathcal{V}_{acc}, \quad (2)$$

where  $\rho(x, t)$  is the traffic density,  $u(x, t)$  the average speed, at time  $t$  and space  $x$  and  $q = \rho u$  is the traffic flow. In (2) we have introduced the modeling of ACC and CACC cars via terms  $p\mathcal{V}_{acc}$  and  $[1 - pF(\rho)]$ , which will be explained later. For  $p = 0$  the original GKT model equations for manually driven cars are obtained. Further in (2),  $\theta = A(\rho)u^2$  is a pressure-like term, with  $A(\rho)$  being a variance factor given by the Fermi function as  $A(\rho) = A_0 +$

<sup>1</sup>School of Production Engineering & Management, Technical University of Crete, Chania 73100, Greece adelis@science.tuc.gr

<sup>2</sup>School of Production Engineering & Management, Technical University of Crete, Chania 73100, Greece jnikolo@dpem.tuc.gr

<sup>3</sup>School of Production Engineering & Management, Technical University of Crete, Chania 73100, Greece markos@dssl.tuc.gr

$\delta A \left[ 1 + \tanh \left( \frac{\rho - \rho_{cr}}{\delta \rho} \right) \right]$  in which,  $\rho_{cr}$  is the critical density,  $A_0$  and  $A_0 + 2\delta A$  the variance pre-factors between free and congested traffic; while  $\delta \rho$  denotes the width of the transition region. Typical range of values for the constants  $A_0$ ,  $\delta A$  and  $\delta \rho$ , along with the typical ranges of the other parameters for this model can be found, for example, in [13], [4], [7], [8], [14], [1], [2]. The model includes a traffic relaxation term aiming to keep flow in equilibrium, with  $V_e^* \equiv V_e^*(\rho, u, \rho_a, u_a)$  being the, non-local and dynamic, equilibrium speed with  $\tau$  being a relaxation time.  $V_e^*$  depends on the non-local density  $\rho_a$  and mean speed  $u_a$  and is defined as

$$V_e^* = u_{\max} \left[ 1 - \frac{\theta + \theta_a}{2A(\rho_{\max})} \left( \frac{\rho_a T}{1 - \rho_a/\rho_{\max}} \right)^2 B(\delta u) \right]. \quad (3)$$

According to (3),  $V_e^*$  is given by the maximum velocity  $u_{\max}$ , reduced by a term that reflects necessary deceleration maneuvers. Both  $\rho_a$  and  $u_a$  are computed at an anticipated location  $x_a = x + \gamma(1/\rho_{\max} + T \cdot u)$  with  $T$  being the average time-headway and  $\gamma$  a scale factor.  $B(\delta u)$  is a Boltzmann interaction factor for  $\delta u = (u - u_a)/\sqrt{\theta + \theta_a}$ , defined as

$$B(z) = 2 [zN(z) + (1 + z^2)E(z)]$$

with  $N(z) = e^{-z^2/2}/\sqrt{2\pi}$  and  $E(z) = \int_{-\infty}^z N(y)dy$ , and describes the dependence of the braking interaction on the dimensionless velocity difference  $\delta u$  between the actual location  $x$  and the anticipation location  $x_a$ . The non-local relaxation term from (3) is forwardly directed and, therefore, is considered to be more realistic compared to other models.

Finally, and following [14], [2], the source term  $r_{rmp}$  in the continuity equation (1) denotes the effective source density from on-ramps (or off-ramps) with merging (diverging) length  $l_{rmp}$  and inflow  $q_{rmp} > 0$  from (or outflow  $q_{rmp} < 0$  to) the ramp, and is given as  $r_{rmp}(x, t) = q_{rmp}(t)/l_{rmp}$  for  $x$  within merging (diverging) zones and zero elsewhere. Moreover, term  $h_{rmp}$  in (2) describes changes of the macroscopic local flow by assuming that on-ramp vehicles merge to the main road at speed  $u_{rmp} < u$  and, conversely, that drivers reduce their speed to  $u_{rmp}$  before leaving the main road. Hence, this term is given as  $h_{rmp}(x, t) = u \cdot r_{rmp} + (u_{rmp} - u)|r_{rmp}|$ .

Next, the novel approach presented in [2] and [9] for modeling ACC and CACC effects in the GKT model equations is briefly described. The modeling is performed through the terms  $p\mathcal{V}_{acc}$  and  $[1 - pF(\rho)]$  in (2). One major difference between this new approach compared to other macroscopic approaches, e.g. those in [6], [8], [7], is that the above terms contribute to the non-local relaxation term in the model equations. Moreover, the *time-gap parameter*, which is an important characteristic of ACC systems, is explicitly taken into account. The ability to explicitly define the time-gap, i.e. the time distance between the rear bumper of the preceding vehicle and the front bumper of the following one, enables the model to simulate ACC/CACC flows with different time-gap settings, which lead to different dynamic behavior and equilibrium capacities.

This novel approach was derived on the basis of the control objectives that an ACC system should follow, in accordance to [11]. These are, to travel with the maximum speed, set by the driver, in cases where no leading vehicles exist in the range covered by the sensors, or leading vehicles exist within range but their velocities are higher than the maximum speed set by the user (*speed control mode*); to maintain vehicle speed equal to the speed of the leading vehicle at a specified distance, when the leading vehicle is in range and its speed is lower than the maximum speed set by the driver (*gap control mode*); and to achieve transitions between the two aforementioned objectives as smooth as possible, in order not to cause discomfort to the passengers due to abrupt accelerations or decelerations. These objectives are satisfied here based on the following modeling assumptions:

(a) For densities clearly below a threshold  $\rho_{acc}$  (being lower than or equal to  $\rho_{cr}$ ) the additional terms in the model have no effect, as it is supposed that (on average) the drivers set their maximum speeds (or react) as in a manual manner, i.e. as the GKT model describes (emulating in that way the speed control mode). In the region around  $\rho_{acc}$ , a smooth but fast transition between the previous case and the ACC/CACC-controlled situation takes place, described using again a Fermi-type function  $F(\rho) = 0.5 \left[ 1 + \tanh \left( \frac{\rho - \rho_{acc}}{\Delta \rho} \right) \right]$  and to achieve this fast transition, the transition width  $\Delta \rho$  takes values of  $\Delta \rho \approx 0.025\rho_{\max}$ . (b) During the gap-control mode, a constant time-gap  $T^*$  is desired, which is imposed through its corresponding effect on a desired density  $\rho^*$  as

$$\rho^* = \frac{1}{1/\rho_{\max} + T^*u^*}, \quad (4)$$

where the denominator is the desired space headway, with  $1/\rho_{\max}$  reflecting the vehicle length and  $u^* = u(x^*)$  is the speed of the preceding vehicle, computed at position

$$x^* = x + \gamma^*(1/\rho_{\max} + T^* \cdot u), \quad \gamma^* \in [1, 2].$$

The desired speed relaxes to the speed of the preceding vehicle  $u^*$  after a relaxation time  $\tau^*$ . As a result, the corresponding source term can be modeled for ACC vehicles as:

$$\mathcal{V}_{acc}(\rho, u, \rho^*, u^*) = F(\rho) \left( \frac{\rho^*u^* - \rho u}{\tau^*} \right). \quad (5)$$

In [5] it was demonstrated that the minimum time-gap that can be achieved by ACC vehicles is 0.8s. In general, indicative values used for ACC traffic are  $T^* \in [0.8, 2.2]s$ , following [ISO 15622, 2010] standards, and  $\tau^* \approx 1s$ .

For V2V CACC vehicles a similar approach is used, but the corresponding source term takes into account the speeds of more than one preceding vehicles, with a different time relaxation for each one of them. The ability for the system to look downstream increases the smoothing effect of the corresponding source term. Furthermore, this additional information from far downstream allows for the use of lower values of time gaps, e.g. as low as  $T^* = 0.6s$ , without compromising safety [11], [12]. As reduced time gaps are only achievable between vehicles that are equipped with

the CACC technology the penetration rate for these systems plays an important role. Thus, for CACC traffic

$$\mathcal{V}_{cacc}(\rho, u, \rho^*, u^*) = F(\rho) \sum_{i=1}^M \left( \frac{\rho^* u_i^* - \rho u}{\tau_i^*} \right) \quad (6)$$

where  $u_i^* = u(x_i^*)$  with  $x_i^* = x + i \cdot \gamma^*(1/\rho_{max} + T^* \cdot u)$ ,  $i = 1, \dots, M$ , and

$$\rho^* = \frac{1}{1/\rho_{max} + T^* u_1^*}.$$

The parameter values used here for CACC traffic are  $M = 3$  with  $[\tau_1^*, \tau_2^*, \tau_3^*] = [2, 3, 6]$ .

In the present work we further extend the above formulation so as to include and study the effect of the penetration rate of ACC and CACC vehicles to the traffic flow. Based on the observation that in some situations, the macroscopic dynamics of microscopic models with heterogeneous vehicles/drivers is essentially that of identical vehicles/drivers with parameters equal to the mean of the heterogeneous vehicle/driver population, we set  $p \in (0, 1)$ , to represent the corresponding penetration rate. We note that, in [2] and [9] only the 100% penetration rate case, i.e.  $p = 1$ , was investigated.

To numerically approximate system (1)-(2), we apply a higher-order finite volume relaxation scheme. The spatial discretization is based on a fifth-order Weighted Essential Non-Oscillatory-type interpolant approach, while for the temporal discretization an implicit-explicit (IMEX) Runge-Kutta splitting was considered. The superiority and performance of this higher-order scheme, compared to low-order ones, in traffic flow simulations has been recently demonstrated in [1] and [2] where a detailed presentation of the spatial and temporal discretizations can be found.

### III. NUMERICAL SIMULATIONS AND DISCUSSION

To study the effect of different penetration rates for ACC or CACC vehicles we consider two test cases. The first is for traffic flow on a circular homogeneous freeway where we aim to examine the formation of traffic instabilities with respect to a perturbation introduced in the flow field. The second test case is the simulation of a freeway with an on-ramp i.e. a potential bottleneck. For brevity, we present results only with time-gap  $T^* = 1.2s$  for ACC and  $T^* = 1s$  for CACC. We note here that these values for  $T^*$  correspond to a more conservative driving behavior, compared to lower values that correspond to more aggressive driving behavior. Usually, vehicles with ACC or CACC have discrete time gap settings, which the driver can select based on his or her perception of the system's capabilities.

#### A. Homogeneous Traffic with a Localized Perturbation

We assume a traffic flow on a ring road of length  $L = 10$  km. Following [13], [4], [8], [1], [2], we consider a dipole-like initial variation of the average density  $\bar{\rho}$  given as  $\rho(x, 0) = \bar{\rho} + \Delta\rho \left[ \cosh^{-2}(D) - \frac{x^+}{x} \cosh^{-2}(E) \right]$  where  $D = (x - x_0)/x^+$  and  $E = (x - x_0 - \Delta x_0)/x^-$  with  $x^+ = 201.5$

and  $x^- = 805$  m and  $\Delta x_0 = x^+ + x^-$ . The initial flow is assumed in local equilibrium. The induced perturbation leads to instabilities for given values of  $\bar{\rho}$ . The ring road was discretized with 400 segments in the finite volume scheme. The model parameters used in the simulations were  $u_{max} = 110$  km/h,  $\rho_{max} = 160$  veh/km,  $\rho_{cr} = 0.27\rho_{max}$ ,  $\tau = 35s$ ,  $A_0 = 0.008$ ,  $\delta A = 0.02$ ,  $\delta\rho = 0.05\rho_{max}$ ,  $T = 1.8$  s and  $\gamma = 1.2$ . Simulations are reported up to a final time of 1200s. The scenario presented here is for  $\bar{\rho} = 35$  veh/km and  $\Delta\rho = 6$  veh/km. A cascade of traffic jams emerges, i.e. stop-and-go waves, as can be seen from the spatio-temporal evolution for the density in Fig. 1 for manual cars, i.e.  $p = 0$ .

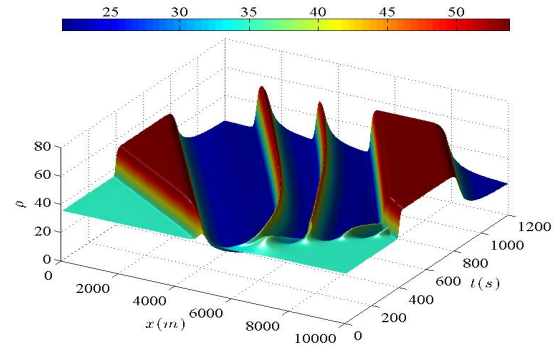


Fig. 1. Density evolution for manual cars for  $\bar{\rho} = 35$  and  $\Delta\rho = 6$

The effect of different penetration rates of ACC or CACC vehicles is presented in Figs 14-17. The values for  $\rho_{acc} = 0.9\rho_{cr}$  and  $\gamma^* = 1$  were used. As it can be observed, even for a 50% rate the mixed ACC traffic is still in the unstable regime, but tends to become uncongested. Increasing the ACC penetration rate results in more stable traffic with less number of waves and smaller wave amplitude. For CACC traffic the initial perturbation rapidly fades out with time for a penetration rate between 20-30%, leading to a homogeneous traffic. Referring to Fig. 6, it is important to note the increased traffic flow rate along the total length of the ring road for ACC and CACC traffic, which is more pronounced for CACC traffic, mainly as a result of the imposed desired time-gap.

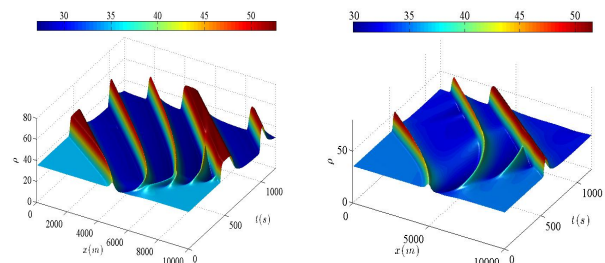


Fig. 2. Density evolution: 10% penetration rate of ACC (left) and CACC (right)

#### B. Flows from an on-ramp

In a first example, we simulate the traffic on a single-lane freeway of  $L = 20$  km with open boundaries for a total of

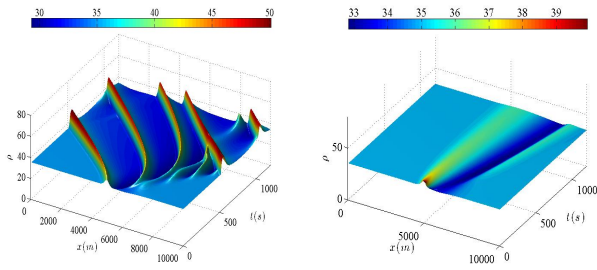


Fig. 3. Density evolution: 20% penetration rate of ACC (left) and CACC

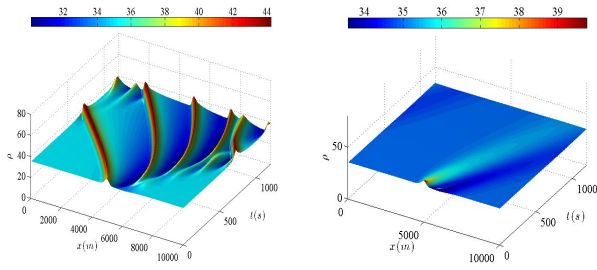


Fig. 4. Density evolution: 30% penetration rate of ACC (left) and CACC

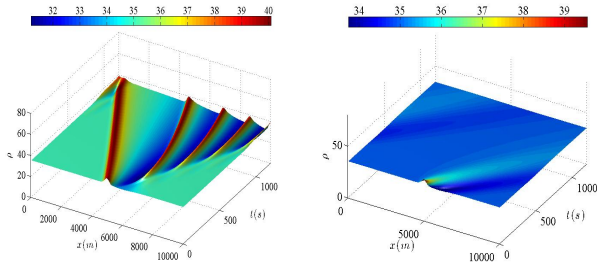


Fig. 5. Density evolution: 50% penetration rate of ACC (left) and CACC

90 minutes. Imposing an initial homogeneous equilibrium traffic flow  $q_f = 1800$  veh/h, simulations are performed for an on-ramp inflow  $q_{rmp} = 250$  veh/h of length  $l_{rmp} = 400$  m located at  $x_{rmp} = 12$  km with a merging zone for  $x \in [x_{rmp} - l_{rmp}/2, x_{rmp} + l_{rmp}/2]$ . For simplicity, we assume that  $u_{rmp} \approx u$  in the  $h_{rmp}$  term in (2). Different traffic states, i.e. congestion patterns, may develop close to bottlenecks caused by on-ramps in a freeway, see for example [4], [14], [2]. The model parameters used in the simulations are,  $u_{max} = 110$  km/h,  $\rho_{max} = 160$  veh/km,  $\rho_{cr} = 0.25\rho_{max}$ ,  $\tau = 35$  s,  $A_0 = 0.008$ ,  $\delta A = 0.01$ ,  $\delta \rho = 0.05\rho_{max}$ ,  $T = 1.8$  s,  $\gamma = 1.2$ ,  $\rho_{acc} = \rho_{cr}$  and  $\gamma^* = 1$ . The traffic density evolution for manual traffic is presented in Fig. 7. Due to the inflow from the on-ramp, the total flow to the merge region is over the equilibrium capacity resulting in an Oscillating Congested Traffic (OCT) flow upstream of the ramp, [4]. In Figs 8-12 the spatio-temporal evolution of density for different penetration rates of ACC/CACC vehicles is presented. Even at a small penetration rate, ACC traffic becomes non-oscillatory upstream of the ramp, but now a Synchronized Homogeneous Congested Traffic (HCT), [4], region slowly develops upstream. When increasing the penetration rate, the jump front moves slower, and the level of the congestion caused by the on-ramp inflow

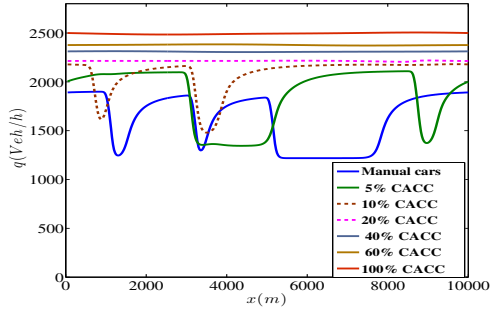
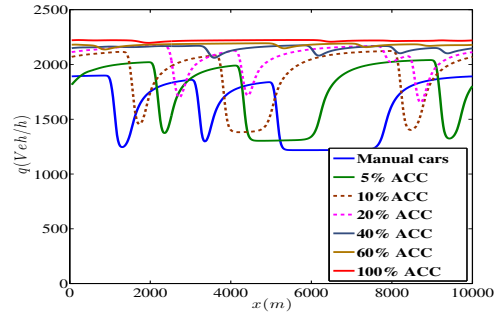


Fig. 6. Flow at  $t = 1200s$  for different penetration rates for ACC (top) and CACC traffic flows (bottom)

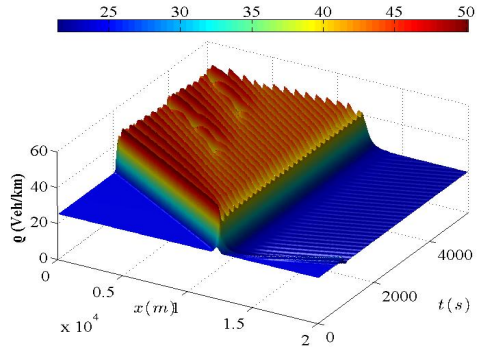


Fig. 7. Density evolution close to an on-ramp for manual cars for  $q_{rmp} = 250$  veh/h

is reduced. For the CACC traffic, the upstream congestion completely disappears at a 30% rate, and a more pronounced increase in the flow rate (capacity) is established. The outflow from the bottleneck, measured downstream of the on-ramp, is improved significantly with the increasing penetration of ACC/CACC vehicles, as shown in Fig. 13. As the activated bottleneck is characterized by a capacity drop, the inclusion of the space-cap principle in our ACC/CACC approach manages to mitigate (or even eliminate) the capacity drop at the bottleneck.

In a second example, we simulate the traffic on a single-lane freeway of  $L = 15$  km with open boundaries for a total of 160 minutes. The initial homogeneous equilibrium traffic flow is  $q_f = 1650$  veh/h with an on-ramp inflow  $q_{rmp} = 200$  veh/h and  $l_{rmp} = 400$  m located at  $x_{rmp} = 10$  km. Stationary conditions are obtained in the first 20 minutes then, we introduce a perturbation of amplitude  $\delta q_{rmp} = 300$  veh/h by

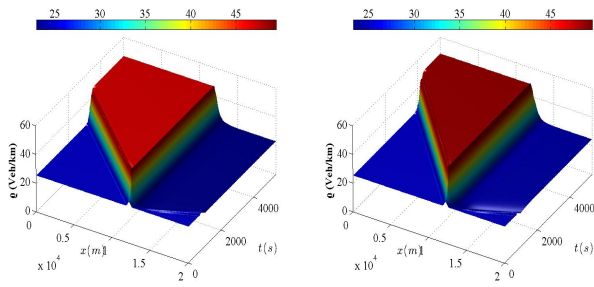


Fig. 8. Density evolution: 10% penetration rate of ACC (left) and CACC (right)

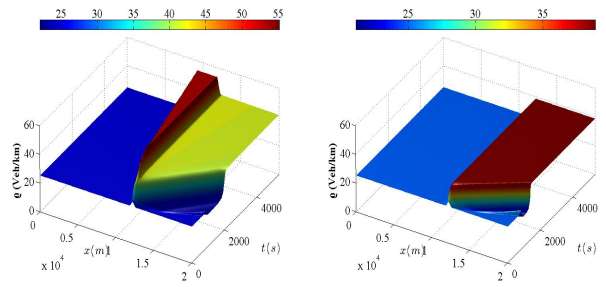


Fig. 12. Density evolution: 50% penetration rate of ACC (left) and CACC (right)

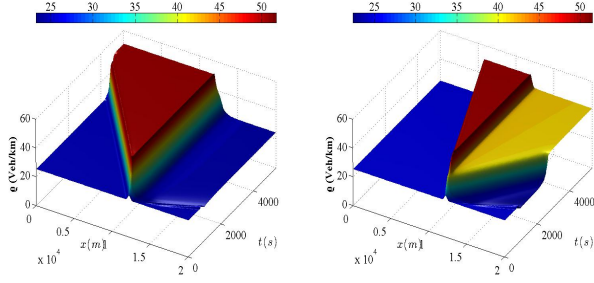


Fig. 9. Density evolution: 20% penetration rate of ACC (left) and CACC (right)

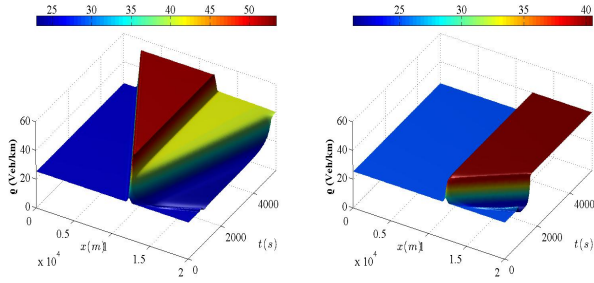


Fig. 10. Density evolution: 30% penetration rate of ACC (left) and CACC (right)

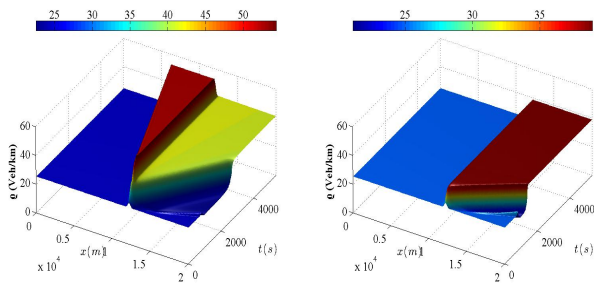


Fig. 11. Density evolution: 40% penetration rate of ACC (left) and CACC (right)

linearly increasing the ramp flow up to  $q_{rmp} + \delta q_{rmp}$  at  $t = 35$  minutes and decreasing it again to  $q_{rmp}$  by  $t = 50$  minutes. The perturbation triggers a synchronized congestion growing upstream of the on-ramp. Then at  $t = 90$  minutes the main flow is reduced to  $q_f = 800$  veh/h which causes the traffic to return to free flow after 60 min. The resulting spatiotemporal evolution of the density can be seen in Fig. 14.

In Figs 15-17 the spatio-temporal evolution of density for

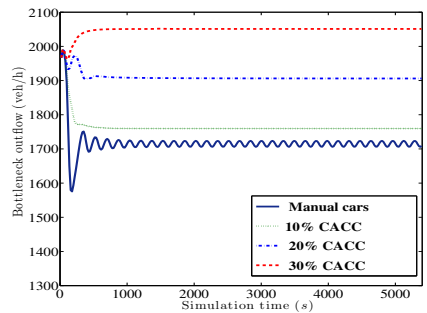
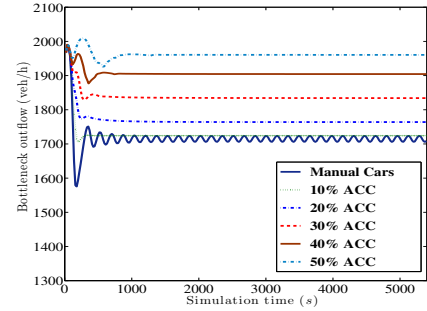


Fig. 13. Effects on the bottleneck capacity, at  $x = 12.2$  km, for different penetration rates for ACC (top) and CACC flow (bottom)

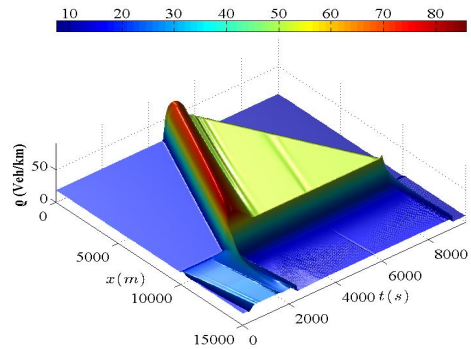


Fig. 14. Density evolution close to an on-ramp for manual cars for  $q_{rmp} = 200$  veh/h and  $\delta q_{rmp} = 300$  veh/h

different penetration rates of ACC and CACC is presented. When increasing the penetration rate, the congestion propagates slower upstream of the on-ramp, and traffic returns to free flow much earlier. Again, for the CACC traffic the upstream congestion completely disappears at a 30%

penetration rate avoiding the traffic breakdown completely in this scenario.

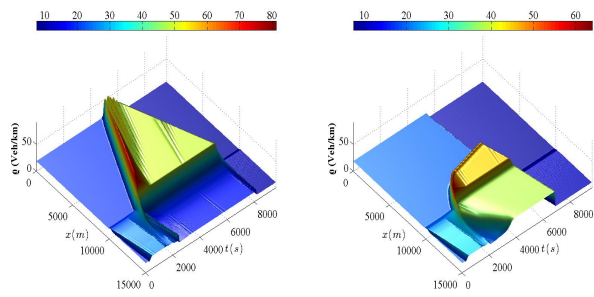


Fig. 15. Density evolution: 10% penetration rate of ACC (left) and CACC

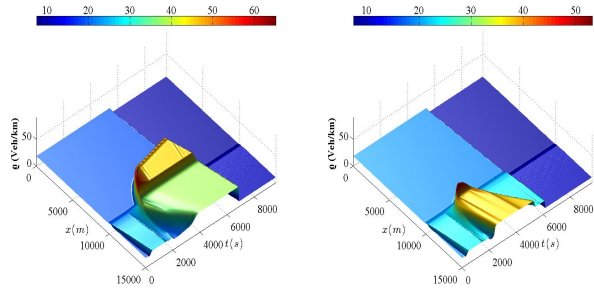


Fig. 16. Density evolution: 20% penetration rate of ACC (left) and CACC

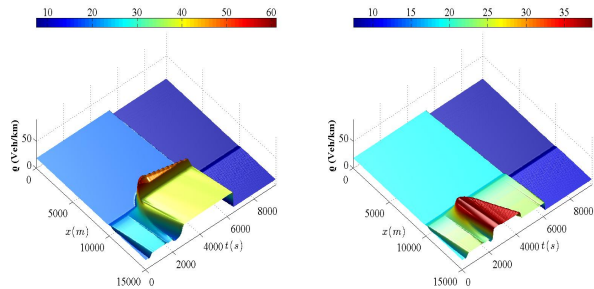


Fig. 17. Density evolution: 30% penetration rate of ACC (left) and CACC

#### IV. CONCLUSIONS

A numerical investigation of the characteristics of mixed, manual and ACC or V2V CACC traffic, has been presented. The contribution of the penetration rate of ACC or CACC vehicles to traffic dynamics has been investigated. A macroscopic approach to model the dynamics of ACC and CACC traffic flows was first given which is based on the introduction of a relaxation term in the momentum equation of the GKT model that satisfies the time-gap principle of ACC systems. The relaxation time is distributed over multiple vehicles in the CACC system whereas in the ACC one the relaxation time is only related to the direct leading vehicle. We have shown numerically that CACC vehicles enhance the stabilization of traffic flow with respect to introduced perturbations compared to ACC ones. The observed enhanced dynamic equilibrium capacity for our CACC system resulted in the suppression of traffic congestion at an on-ramp bottleneck even at a penetration rate of around 30%.

However, to find a global critical penetration rate value, there is a need for much more experiments in different traffic situations and a sensitivity analysis should be performed for the system's parameters such as the time-gap. In our modeling approach it is also possible to incorporate variable time-gap preferences, as can be set by different groups of drivers. This has been left for a future presentation. Time-gap preferences have a significant influence on traffic flow and highway lane capacity. Nevertheless, the results from this study confirm that, if only a fraction of vehicles are equipped with CACC, traffic congestion can be reduced by improving highway capacity and throughput.

#### ACKNOWLEDGMENT

This research was supported by TRAFFIC MANAGEMENT for the 21st century (TRAMAN21) ERC Advanced Investigator Grand under the European Union's Seventh Framework Program (FP/2007-20013).

#### REFERENCES

- [1] A.I. Delis, I.K. Nikolos and M. Papageorgiou, "High-resolution numerical relaxation approximations to second-order macroscopic traffic flow models", *Transportation Research Part C: Emerging Technologies*, vol. 44, pp. 318-349, 2014.
- [2] A.I. Delis, I.K. Nikolos and M. Papageorgiou, "Adaptive cruise control for a macroscopic traffic flow model: development and numerical solution", *Computers and Mathematics with Applications*, vol. 70, pp. 1921-1947, 2015.
- [3] A. Kesting, M. Treiber, M. Schönhof and D. Helbing, "Adaptive cruise control design for active congestion avoidance", *Transportation Research Part C: Emerging Technologies*, vol. 16, pp. 688-683, 2008.
- [4] D. Helbing, A. Hennecke, V. Shvetsov and M. Treiber, "MASTER: Macroscopic traffic simulation based on a gas-kinetic, non-local traffic model", *Transportation Research Part B: Methodological*, vol. 35, pp. 183-211, 2001.
- [5] G. Marsden G., M. McDonald and M. Brackstone, "Towards an understanding of adaptive cruise control", *Transportation Research Part C: Emerging Technologies*, vol. 9, pp. 3351, 2001.
- [6] D. Ngoduy, S.P. Hoogendoorn and R. Liu, "Continuum modeling of cooperative traffic flow dynamics", *Physica A*, vol. 388, pp. 2705-2716, 2009.
- [7] D. Ngoduy, "Application of gas-kinetic theory to modeling mixed traffic of manual and ACC vehicles", *Transportmetrica*, vol. 8, pp.43-60, 2012.
- [8] D. Ngoduy, "Instability of cooperative adaptive cruise control traffic flow: A macroscopic approach", *Commun. Nonlinear Sci Numer. Simulat.*, vol. 18, pp. 2838-2851, 2013.
- [9] I.K. Nikolos, A.I. Delis and M. Papageorgiou, "Macroscopic Modeling and Simulation of ACC and CACC Traffic", Proc. 18th IEEE International Conference on Intelligent Transportation Systems (ITSC 2015), Sept. 2015, 7313436, pp. 2129-2134.
- [10] K.N. Porfyri, I.K. Nikolos, A.I. Delis and M. Papageorgiou, "Stability Analysis of a Macroscopic Traffic Flow Model for Adaptive Cruise Control Systems", Proc. ASME. 57557, Vol. 12: Transportation Systems, Nov. 2015, pp. V012T15A002; 9 pages, doi:10.1115/IMECE2015-50977.
- [11] S.E. Shladover, D. Su and X.-T. Lu, "Impacts of Cooperative Adaptive Cruise Control on Freeway Traffic Flow", *Transp. Res. Rec. J. Transp. Res. Board*, No. 2324, pp. 6370, 2012.
- [12] S.E. Shladover, C. Nowakowski, X.-T. Lu and R. Ferlis, "Cooperative Adaptive Cruise Control: Definitions and Operating Concepts", *Transp. Res. Rec. J. Transp. Res. Board*, No. 2489, pp. 145-152, 2015.
- [13] M. Treiber, A. Hennecke and D. Helbing, "Derivation, properties, and simulation of a gas-kinetic-based, non-local traffic model", *Physical Review E - Statistical Physics, Plasmas, Fluids, and Related Interdisciplinary Topics*, vol. 59, pp. 239-253, 1999.
- [14] M. Treiber and A. Kesting, *Traffic flow dynamics: Data, models and simulation*, Springer, 2013.